JOURNAL OF GEOPHYSICAL RESEARCH, VOL. 105, NO. D22, PAGES 26,971–26,989, NOVEMBER 27, 2000

Trends in tropospheric aerosol loads and corresponding impact on direct radiative forcing between 1950 and 1990: A model study

Ina Tegen,[1] Dorothy Koch,[2,3] Andrew A. Lacis,[3] and Makiko Sato[2,3]

Abstract. Global aerosol optical thicknesses and radiative properties need to be known for the study of decadal temperature change. Aerosol distributions have been developed from global transport models for a mixture of sulfate and carbonaceous aerosols from fossil fuel burning, including also contributions from other major aerosol types such as soil dust and sea salt. Between the years 1950 and 1990 the aerosol distributions change due to changes in emissions of SO_2 and carbon particles from fossil fuel burning. The optical thickness of fossil fuel derived aerosols increased by nearly a factor of 3 during this period, with particularly strong increase in eastern Asia. In countries where environmental laws came into effect since the early 1980s (e.g., United States and western Europe), emissions and consequently aerosol optical thicknesses did not increase considerably after 1980, resulting in a shift in the global distribution pattern. In addition to the optical thickness, aerosol single scattering albedos may have changed during this period due to different trends in absorbing black carbon and reflecting sulfate aerosols. However, due to uncertainties in the emission trends, which are especially large in the case of carbonaceous aerosols, such change cannot be determined with any confidence. Radiative forcing of this aerosol distribution is calculated for several scenarios. Uncertainties in the contribution of the strongly absorbing black carbon aerosol leads to a range in top-of-atmosphere forcings of $\approx$ -0.5 to +0.1 Wm^{-2}.

1. Introduction

Climate forcing by anthropogenic tropospheric aerosols remains one of the largest uncertainties in climate variability and climate change studies [e.g., *Hansen et al.*, 1997, 1998]. Aerosols can influence the radiation budget directly by scattering and absorbing solar and thermal radiation (direct radiative forcing), or indirectly, by changing the number of cloud condensation nuclei, which may lead to changes in the albedo and lifetime of clouds (indirect radiative forcing). In this study, we only consider the direct forcing by tropospheric aerosols.

Natural and anthropogenic aerosols exhibit strong geographic and seasonal variations, which produce a globally uneven pattern of radiative forcing (compared to greenhouse gases). Moreover, there is a large uncertainty in aerosol radiative parameters (particularly single scattering albedo) which results in even greater uncertainty of the (direct) radiative forcing. The anthropogenic aerosols that are suspected to have the largest impact on climate are sulfate (which scatters solar radiation, causing regional cooling), and black carbon aerosol (BC) which is strongly absorbing at solar wavelengths, causing atmospheric heating. The magnitude and sign of the aerosol forcing depend on both aerosol optical thickness and single scattering albedo, which is determined by the aerosol distribution and chemical composition.

In the future, new satellite instruments are expected to improve our understanding of global aerosol properties. However, for now the possibilities of deriving distributions of aerosol properties from satellite observations are limited. So far, estimates of tropospheric aerosol forcing and climate effects rely on aerosol distributions derived from transport models. Most estimates of this kind exist for anthropogenic sulfate aerosols [e.g., *Charlson et al.*, 1991; *Kiehl and Briegleb*, 1993; *Kiehl and Rodhe*, 1995; *Roeckner et al.*, 1995]. Recently, several studies investigated the optical properties and radiative effects of a mixture of sulfate and carbonaceous aerosols [*Haywood et al.*, 1997; *Haywood and Ramaswamy*, 1998; *Schult et al.*, 1997; *Penner et al.*, 1998; *Mhyre et al.*, 1999]. The change in top-of-atmosphere

[1]Max Planck Institute for Biogeochemistry, Jena, Germany.

[2]Center for Climate Systems Research, Columbia University, New York.

[3]NASA Goddard Institute for Space Studies, New York.

Paper number 2000JD900280.
0148-0227/00/2000JD900280$09.00

(TOA) radiative fluxes caused by this aerosol mixture in these studies ranged from -0.88 to +0.1 Wm^{-2}; this range reflects some of the uncertainties in such estimates.

Those estimates result from taking the difference between radiative fluxes obtained with an aerosol distribution from a reference year and the "preindustrial" case with no anthropogenic aerosols present. However, considerable changes in aerosol distributions may have taken place during the last decades. Since the 1950s, global SO_2 emissions (SO_2 is a precursor of sulfate aerosol) increased considerably with different rates for different countries [e.g., *Lefohn et al.*, 1999]. Not only changes in total aerosol optical thickness but also changes in aerosol composition may have occurred, since SO_2 emissions were considerably curbed in the United States and western Europe since the early 1980s due to environmental regulations like the Clean Air Act. The emissions of black carbon particles may not have been reduced as effectively in those regions, although they may have been reduced by changes in the fossil fuel burning technology. In other parts of the world, like east Asia, SO_2 emissions and therefore presumably sulfate aerosol concentrations increased strongly during the whole period since 1950.

Here we present an estimate of changes in sulfate, BC, and organic aerosols from fossil fuel burning from 1950 to 1990, together with an estimate of how these changes affect the tropospheric aerosol properties and TOA radiative fluxes. The resulting distributions of tropospheric aerosols are designed for use in climate change studies.

2. Aerosol Distributions

2.1. Aerosol Emissions From Fossil Fuel Burning

2.1.1. Sulfate. Several estimates of global emissions of sulfur dioxide, the precursor for sulfate aerosol, are available. A detailed emission scenario for the year 1985 has been developed by *Benkovitz et al.* [1996]. *Dignon and Hameed* [1989] estimated global sulfur emission trends from 1860 to 1980 by correlating sulfur emission data with liquid and solid fossil fuel use data for countries that are members of the Organization of Economic Cooperation and Development (OECD) and non-OECD countries. A different database of global sulfur emissions, which is used in this investigation, has been developed by *Lefohn et al.* [1999], who estimated historical global sulfur emission for the years 1850 to 1990 by using statistical data on fossil fuel use (equaling production plus import minus export with fuel consumption). They computed sulfur emissions for each country by multiplying the net fuel use with the sulfur content of the fuel and by a factor incorporating sulfur retention, thus obtaining sulfur emissions per year and country. Additionally, SO_2 emissions from metal production were taken into account. Specifically, they considered flue gas desulfurization controls in coal burning facilities, as well as low-sulfur coal switching strategies, which were implemented in 1973 in the United States. To obtain higher resolved geographical distributions, we weighted the emission data, which are given by country, with the population density for each country on a 1° by 1° grid. Figure 1 shows the sulfur emissions from

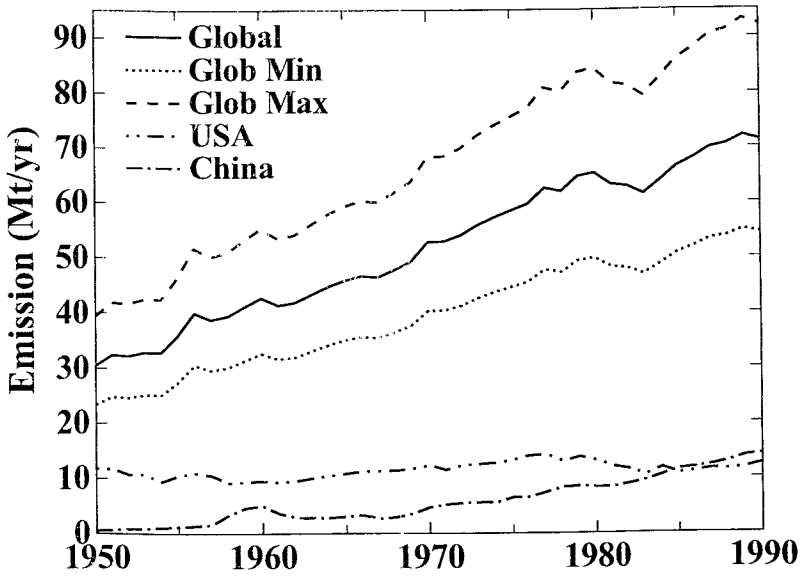

Figure 1. Emissions of SO_2 (in Mt S yr^{-1}) from 1950 to 1990. Shown are global averages, uncertainty ranges, and emissions for the United States and China.

Lefohn et al. [1999] for the global average and for the examples of United States and China for the years 1950 to 1990. While during that period the global increase in sulfur emissions was almost linear, with a drop between 1980 and 1985, the sulfur emissions in China increased more strongly. In the United States, on the other hand, sulfur emissions have slightly decreased since the late 1970s. The sulfur emission trend for countries in western Europe, another major source region, is similar to the trend for the United States. One of the largest uncertainties in this emission database is the actual sulfur content of the fossil fuels. Based on the data given by *Lefohn et al.* [1999], the uncertainty in sulfur emissions is estimated to be 25% in the global mean (see Figure 1), with a range of 5% to 80% for individual countries. Globally, the sulfur emission values for the reference year 1985 from this work agree very well with the widely used sulfur emission data set from *Benkovitz et al.* [1996] (S emissions in 1985 are $\approx$ 65 Mt yr^{-1} in both studies [*Lefohn et al.,* 1999]), although there are some regional differences.

2.1.2. Black carbon. Black carbon aerosol is emitted into the atmosphere by burning of fossil fuel and biomass. For the aerosol trend estimates we only consider fossil fuel emissions. Given the state of current knowledge, global trends in biomass burning aerosol emissions cannot be estimated with any confidence. We used the method described by *Cooke and Wilson* [1996] (CW96) to derive global black carbon (BC) emissions from fossil fuel burning from the United Nations energy statistics database [*United Nations,* 1996]. While the authors extracted global black carbon emissions specifically for the year 1984, we applied a simplified version of their method to the period 1950 to 1994, which is the full period for which data from the UN statistics database are available. CW96 calculated fuel use as the difference of the sum of fuel production and imports and the sum of exports and stock changes for each country. BC emissions were calculated by multiplying the amount of fuel use with emission factors from the literature for domestic and industrial burning for 126 fuel types. In a more recent detailed study of global BC emissions, *Cooke et al.* [1999] took into account the level of development for calculating emissions from a country, thus updating the CW96 BC emissions database. However, considering the large uncertainties in BC emissions, we used the simpler CW96 method. The results from applying this method can be regarded as an upper limit for global BC emissions, since the emission factors used in the more recent study are lower. Also, *Bond et al.,* [1998, 1999b] found emission factors of light-absorbing particles from a lignite power plant that were lower by an order of magnitude than the factor used in the *Cooke et al.* [1999] study.

In the simplified version, we considered only the consumption of hard coal, brown coal, and diesel, since the burning of these fuels are the main sources for BC aerosol. Following CW96, we assumed emission factors of 10 g BC kg^{-1} fuel for domestic burning of hard coal and brown coal, 1 g BC kg^{-1} fuel for industrial coal burning, 2 g BC kg^{-1} for domestic and 0.7 g BC kg^{-1} for industrial diesel fuel burning. Information about the percentage of domestic versus industrial fuel use were missing for several countries in the UN energy statistics. Therefore all countries were grouped into nine regions with similar geographic location and political/economical systems. Those were Africa, Centrally Planned Asia, Centrally Planned Europe, Developing America, Far East, Middle East, North America, Oceania, and Western Europe, as defined by *Boden et al.* [1996]. Average emission factors were calculated for the countries in each region and the years for which the information on relative contribution of domestic and industrial burning to the use of the individual fuel types was available. Those were then applied for those countries and years where only information about total fuel use was available. These emission factors in effect replace the combined emission for industrial and domestic fuel burning used by CW96. This simplification of the method of CW96 results in global BC emissions of 8.3 Mt yr^{-1} for the year 1984, which agrees very well with the emission of 8.0 Mt yr^{-1} calculated by CW96. Since the emission factors used in both calculations were the same, this agreement indicates that the simplifications in the method were justified, not that the results are necessarily realistic. The newer estimate by *Cooke et al.* [1999] results in a lower global annual emission of BC aerosol of 6.4 Mt yr^{-1}.

The resulting trend in BC emissions reflects the trend in the total fossil fuel use, and the shifts between the use of coal and diesel fuel. Since the percentage of fuel use in domestic versus industrial sectors was not reported for years before 1970, we assumed the same relation between domestic and industrial fuel burning as for the average of the years 1970 to 1994. An additional decrease in BC emissions may have occurred due to shifts from domestic to industrial use of the individual fuel types. To test the implications of these shifts on BC emissions, we estimated this trend for most regions by extrapolating the percent burning in the industrial sector that was found in the period 1970 to 1990 back to the year 1950. For those regions (specifically Western Europe, which experienced a shift from domestic to industrial burning) this results in a reduced emission increase. Considering the uncertainties in emission factors and the possible effects of changes in technology, this difference was found to be insignificant.

Figure 2 shows the resulting trend for global BC emissions. Also shown are the examples of BC emissions for the United States, China, and Germany. The resulting trend in global BC emission is steeper than linear. In

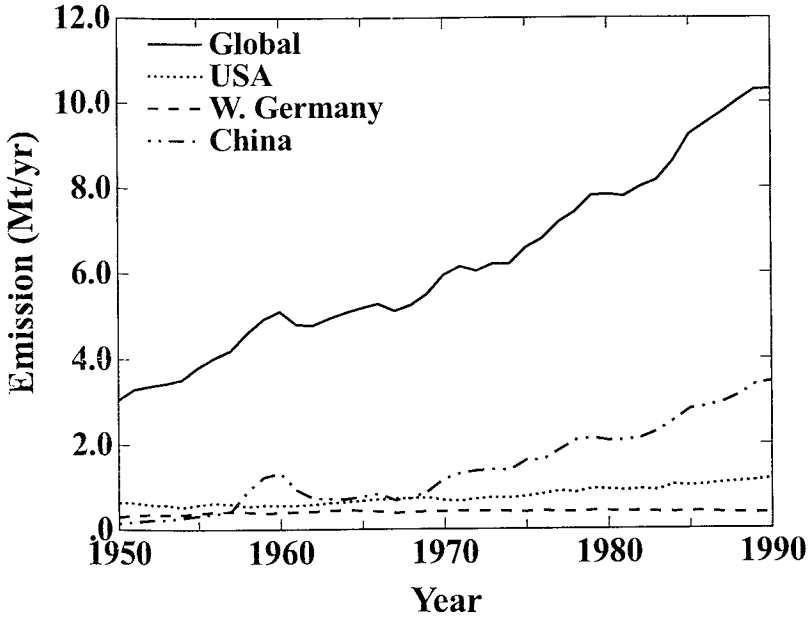

Figure 2. Emissions of BC (in Mt C yr^{-1}) from 1950 to 1990. Shown are global averages and emissions for the United States, China, and Germany.

both United States and China, BC emissions increased over the whole period 1950 to 1990.

Emission factors from the CW96 study were high compared to the revised study by *Cooke et al.* [1999]. Therefore we regarded the results for global BC emission obtained by this method as an upper limit. To take into account the uncertainties in BC emissions, in the following we estimate the effect of reducing BC emissions by 50% and 80%, respectively.

As for SO_2 emissions, the distribution of BC emissions on a 1° by 1° map was obtained by weighting the emissions that are calculated for each country with the population density distribution in each country.

2.1.3. Organic aerosol. Organic carbonaceous aerosol (OC) is the less absorbing, chemically reactive part of the carbon containing aerosol. Organic aerosol can be emitted from fossil fuel burning, from biomass burning, or as natural emissions from plants (e.g., terpenes). For the purpose of estimating an aerosol trend from 1950 to 1990, here we are mainly interested in the trend in organic aerosol emissions from fossil fuel burning. Very little information is available on these emissions, although the recent Tropospheric Aerosol Radiative Forcing Observational Experiment (TARFOX) showed a strong contribution of organic aerosols to the total aerosol scattering off the coast of the eastern United States [*Hegg et al.*, 1997]. Since even less information on OC emissions and concentrations is available compared to BC aerosol, we obtained OC emissions by multiplying BC emissions by a factor of 4 (as done by e.g. *Liousse et al.* [1996] and *Penner et al.* [1998]). Using this factor, the resulting organic aerosol mass load (derived with a transport model, see below) in the TARFOX area is of the same magnitude as the sulfate content at that location (using the sulfate distribution calculated by *Koch et al.* [1999]). As for the BC emissions, this method results probably an upper limit for global OC emissions, since it is based on the upper limit estimate for BC emissions. Also, some of the organic aerosol detected during the TARFOX campaign may have originated from plant emissions instead of fossil fuel burning. To estimate a lower limit for the organic aerosol emissions from fossil fuel burning is difficult without more constraints. To make an estimate of the full range of uncertainties for OC emissions, we assume the lower limit for OC emissions from fossil fuel burning to be zero.

2.2. Aerosol Distribution and Optical Thickness

2.2.1. Sulfate. From the global emission fields, aerosol distributions are calculated using previously described aerosol transport/chemistry models. The global annual SO_2 emissions were averaged over 10-year periods and resulting aerosol distributions were calculated for the years 1950, 1960, 1970, 1980, and 1990. The sulfate aerosol distributions for individual years were obtained by interpolating the average decadal distribution to obtain the regional distribution. For each year the concentrations were then scaled with the global emissions of SO_2 for that particular year.

Sulfate distributions were obtained with the model of *Koch et al.* [1999], who calculated sulfate chemistry and transport online in the Goddard Institute for Space Studies general circulation model (GISS GCM). The chemistry model includes prognostic H_2O_2 as in-cloud

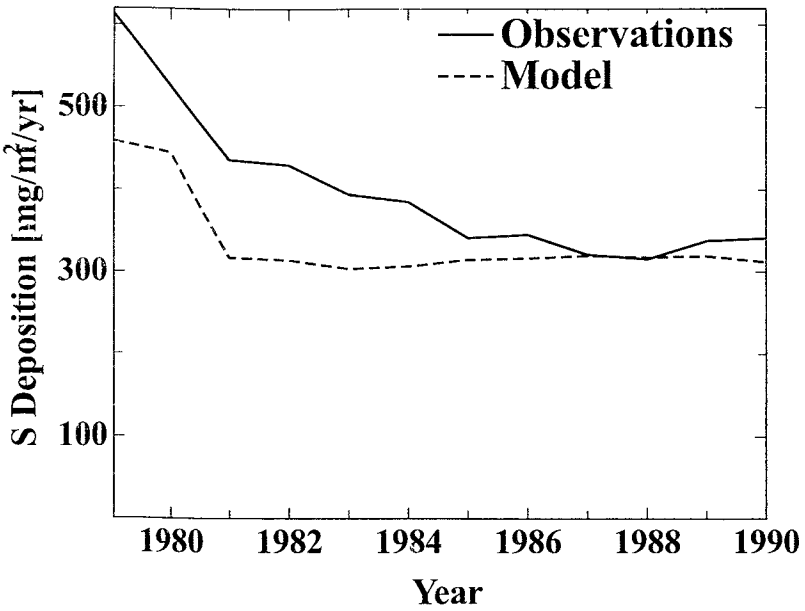

Figure 3. Comparison of modeled sulfur deposition with measurements at NADP in the U.S. sites from 1979 to 1990; deposition fluxes are in mg S m^{-2} yr^{-1}.

oxidant, together with OH, dimethyl sulfide (DMS), methanesulfonic acid (MSA), SO_2 and sulfate. Unlike the sulfate precursor SO_2, the oxidants are kept constant over the years in these calculations. The anthropogenic increase in SO_2 emission translates directly into an increase in sulfate aerosol loads. The GCM was integrated for 6 model years, and the resulting SO_4 concentrations from the last 5 years were averaged. The *Koch et al.* [1999] sulfate model, using SO_2 emissions of *Benkovitz et al.* [1996], has been validated by extensive comparisons with observations of surface concentrations of SO_4 and SO_2, as well as sulfur deposition.

Validating the long-term trend in sulfate concentrations is problematic, since it requires comparison with measurements taken over a multiyear period, ideally more than 10 years. An increasing trend in sulfate concentrations since 1950 can be found in Greenland ice cores [*Mosher et al.*, 1993; *Mayewski et al.*, 1990]. From measurements of sulfate concentration at a Greenland ice core near Dye 3, *Mayewski et al.* [1990] find that the increase in sulfate at this location is most similar to the trend in SO_2 emission increase in the United States (concluding that this is the primary source for sulfate in south Greenland). However, it is difficult to interpret such data from the remote site at Greenland, since those data do not represent hemispherical values. Due to the short lifetime of aerosols, changes in transport and local effects can influence the signal in the ice cores. Recent studies of changes in anthropogenic sulfate concentrations during the past decades in Alpine ice cores [*Schwikowski et al.*, 1999a, 1999b] also show a significant increase since 1950 and decreasing sulfate concentrations from the mid-1970s. This agrees qualitatively with the trend in sulfur emissions in the European countries close to the sampling site.

The decrease in sulfate deposition in the United States is reflected in the observations from the National Acid Deposition Program/National Trends Network (NADP/NTS) assessment for the years 1979 to present [*National Acid Deposition Program*, 1999]. Figure 3 shows a comparison of model results with the observed sulfur deposition fluxes, averaged for the continental United States. The network measurements started in 1979 with 24 stations, the number increased to 181 stations in the year 1996. The modeled sulfur deposition lies below the observations until the mid-1980s, but there is agreement in the trend in sulfur depositions for model and observations. A strong decrease in sulfur deposition exists in the beginning of the 1980s, leveling off in the late 1980s.

In western Europe, long-term sulfate measurements exist from the network of the Cooperative Program for Monitoring and Evaluation of the Long-Range Transmission of Air Pollution in Europe (EMEP) [e.g., *Schaug et al.*, 1987] since the late 1970s for 32 EMEP sites. Figure 4a shows a comparison of sulfate concentration measurements with the model results for 32 EMEP stations, which are subdivided for 17 central European stations (south of 55°N) (Figure 4b) and 15 northern (north of 55°N) stations (Figure 4c). As for the comparison with the NADP measurements, the trend of sulfate concentrations is reproduced over the years, with a decrease between 1980 and 1990. The decreasing trend is stronger for the central European stations, where the model overestimates total sulfate concentrations. On the other hand, the agreement of the model with the observations is very good for the northern European stations. The decreasing trend in sulfate concentrations between 1980 and 1990 is not as strong at those stations, compared to the European average.

The modeled sulfate aerosol mass loads were con-

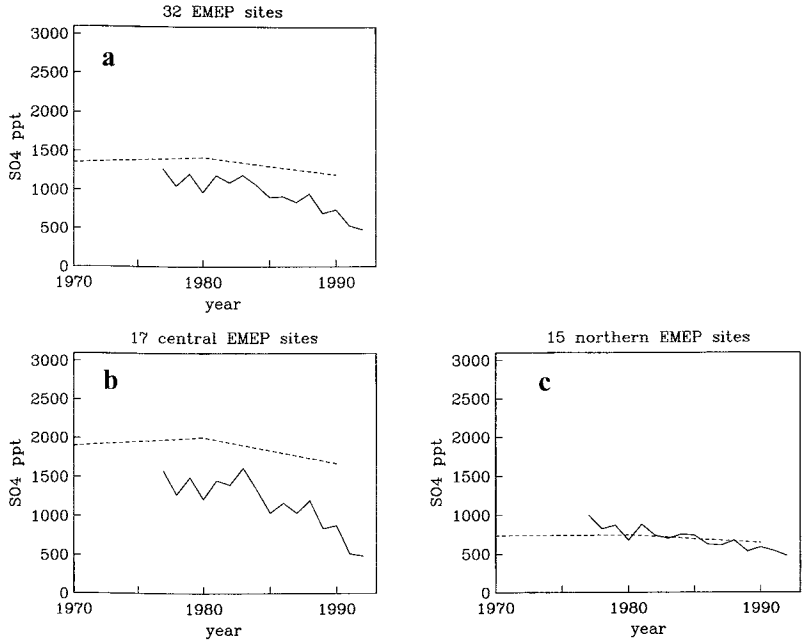

Figure 4. Comparison of sulfate concentration trends in the model with measurements at EMEP sites in Europe. Compared are the trends for (a) all stations and (b) central, and (c) northern European sites separately. For Figures 3 and 4, the station data were averaged over all sites, while the model results were averaged for the corresponding land grid boxes.

verted into aerosol optical thicknesses τ by taking into account the hygroscopic growth of the sulfate particles, using the formulation of *Charlson et al.* [1984] $\tau = mB(\mathrm{RH})$. (Variable m is the sulfate mass load in $\mathrm{g\,m^{-2}}$, $B(\mathrm{RH})= 5\ \mathrm{m^2\,g^{-1}} \times f(\mathrm{RH})$, where $f(\mathrm{RH})$ accounts for the effect of relative humidity (RH) on the optical thickness.) $B(\mathrm{RH})$ is capped at 2.5 for RH> 85%.

In Table 1 the major uncertainty factors for the estimate of sulfate optical thickness are summarized, which are estimated according to *Penner et al.* [1994]. The values given in this table reflect uncertainties in the input parameters or model structure. Additional uncertainties can be caused by neglecting some atmospheric processes and subgrid scale variations. Those latter uncertainties cannot be quantified. The uncertainty factor of 1.4 for sulfate production takes into account the uncertainty in sulfur content of the fossil fuels stated above, as well as the uncertainty in the percentage of sulfur dioxide which is oxidized to sulfate. The latter is derived from the range of results from seven sulfur transport/chemistry models that were cited by *Koch et al.* [1999]. The uncertainty factor of 1.2 of the atmospheric lifetimes of sulfate aerosol results from the same model comparison. It reflects uncertainties in the geographical distribution and deposition. The uncertainty factor of 1.5 for the specific scattering cross section B_s is taken from *Penner et al.* [1994], it reflects the uncertainties in the dependence of B_s on relative humidity.

2.2.2. Black and organic carbon aerosols. Black carbon and organic aerosol distributions were calculated using the GISS tracer transport model. For present-day conditions, the results were described by *Hollrigl* [1997]. The model is based on the GISS aerosol model described by *Tegen and Fung* [1994] for soil dust aerosol. In order to estimate the maximum contribution of carbonaceous aerosol to the tropospheric aerosol load, we assumed BC and OC particles to be insoluble and not being able to form cloud condensation nuclei. Wet removal is by subcloud scavenging. OC may be partly soluble and BC may become coated by sulfate aerosol and consequently become increasingly hygroscopic, which means that wet deposition was probably underestimated by this method. Also, carbonaceous aerosols could be efficiently scavenged in wet convection (which has been shown by measurements during the recent Indian Ocean Experiment (INDOEX) campaign). The underestimate of this process leads to too high remote concentrations of carbonaceous aerosol. On the other hand, the resulting overestimate of OC concentrations in remote regions may be partially offset by the production of secondary OC aerosol downwind of the source areas, which was ignored in these simplified calculations.

Carbonaceous aerosol concentrations from this model using the high emission and low deposition estimates can be regarded as an upper limit. For this case the atmospheric lifetime for BC is $\approx$ 15 days, and the resulting BC mass load is 0.7 $\mathrm{mg\,m^{-2}}$. This is approximately 4 times higher than the estimates from *Liousse et al.* [1996] and *Cooke et al.* [1999]. To construct aerosol scenarios that take into account the uncertainties in emission and wet deposition of carbonaceous

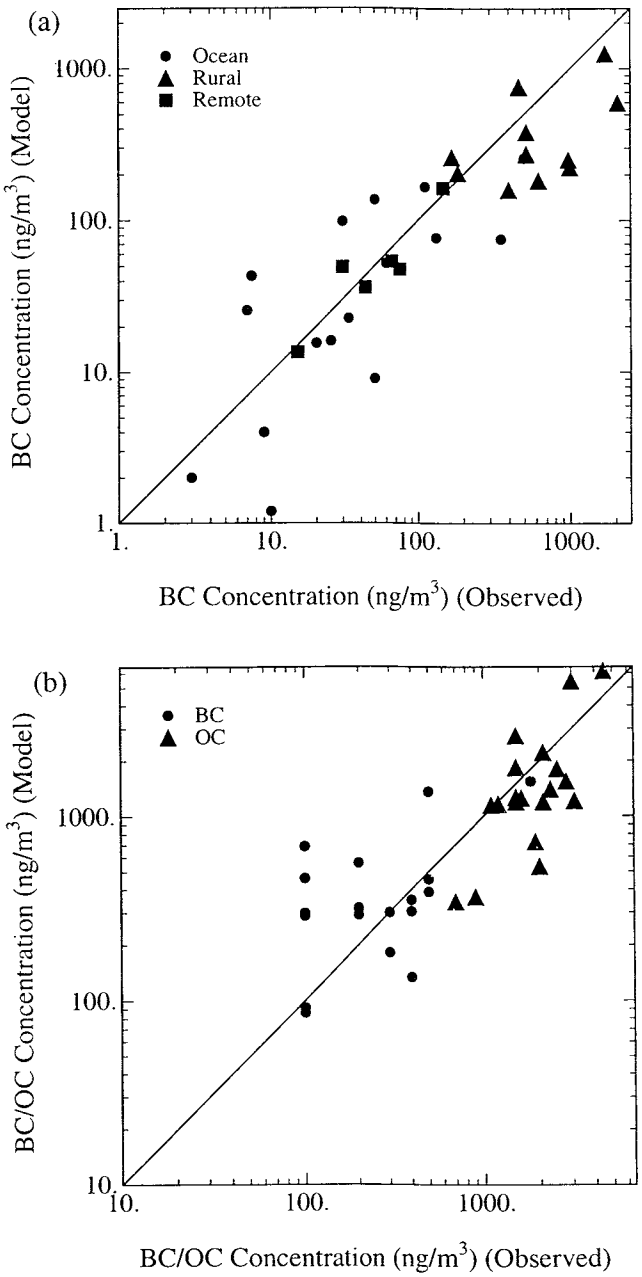

Figure 5. Comparison of modeled BC concentrations with (a) measurements summarized by *Liousse et al.* [1996] (monthly and seasonal means) and (b) modeled BC and OC concentrations measurements from the IMPROVE network sites [*Malm et al.*, 1994] for the case of moderate carbonaceous aerosol (annual means).

aerosols, we decreased the BC load obtained by our model by 50% ("moderate-BC" case) and 80% ("low-BC" case), respectively. Those sensitivity studies approximately cover the range of uncertainties in the atmospheric BC load. For these cases, the OC load was lowered by these factors as well.

Figures 5a and 5b show the comparison of BC concentrations for the moderate-BC case with measurements from various authors, summarized by *Liousse et al.* [1996], and the comparison of BC and OC aerosol concentrations with stations from the Interagency Monitoring of Protected Visual Environments (IMPROVE) network in the United States [*Malm et al.*, 1994], respectively. For Figure 5a, only Northern Hemisphere data were compared to the model results since we were evaluating the BC distribution from fossil fuel emissions and assume biomass burning contribution to be small in these locations. Figure 5a shows reasonable agreement between model results at remote stations. For ocean stations some scattering exists, while for this moderate-BC case the model generally underestimates the BC concentrations at rural stations, at those locations the maximum-BC case gives good agreement. Similarly, for the U.S. stations (which are also "rural" stations) (Figure 5b) the model underestimates BC and OC concentrations for the moderate case; the maximum-BC case would give better agreement.

While for sulfate aerosol some long-term observations exist (which were supported in response to concerns about "acid rain"), long-term measurements of carbonaceous aerosols are very limited. The trend for this aerosol type remains therefore highly uncertain. In a recent study, *Lavanchy et al.* [1999] show the trend in BC and total carbon concentrations in an Alpine ice core for the time period 1755 to 1975. Between the periods of 1945 to 1955 and 1956 to 1965 they find an increase in both BC and total carbon concentrations by 30%. This agrees well with the modeled increase in BC emissions during this time period in Germany, which dominates BC emissions in the countries influencing the sampling site. In the ice core data this increase is followed by a decrease in BC concentrations but unchanged total carbon concentrations until 1975. The calculated BC emissions increase for Germany during this period, while a decrease in carbon aerosol would agree with the estimate in the BC emission trend if the shift between domestic and industrial fossil fuel burning was taken into account (see section 2.1.2). Apart from the assumption that BC emissions from fossil fuel burning was increasing after 1950, the emission trends cannot be validated with information that is currently available.

BC and OC aerosol were converted into optical thicknesses using $\tau = mB$ by using specific extinction cross sections B of 9 $m^2 g^{-1}$ and 8 $m^2 g^{-1}$ [*Liousse et al.*, 1996], respectively. Possible changes in optical thickness due to a change in hygroscopic growth of carbonaceous particles were not taken into account.

Table 1. Parametric Uncertainty Factors in the Calculation of Fossil Fuel Aerosol Forcing

Parameter	Sulfate	BC	BC+OC
Emission/production	1.4	2.3	3.8
Lifetime	1.2	2.0	2.0
B_s	1.5	1.2	2.3
B_a	-	1.3	1.2

Table 1 summarizes the major uncertainty factors for the estimate of BC and total carbonaceous aerosol optical thickness, which are clearly larger than the uncertainty factors for the case of sulfate aerosol. For carbonaceous aerosols the largest uncertainties are in the emission estimates. For BC emissions the uncertainty factor reflects the range assumed for the high-BC and low-BC case, while the uncertainty factor of 3.8 for total carbonaceous aerosol includes a lower limit of fossil fuel OC emissions of zero. The uncertainty factor of 2 for atmospheric lifetime of carbonaceous aerosols covers the range of results of this study and the results cited by *Cooke et al.* [1999]. The uncertainty factors for specific scattering and absorption cross sections (B_s and B_a) are taken from *Penner et al.* [1998], the largest value of 2.3 is given for the total carbonaceous aerosol specific scattering cross section. The overall uncertainty factor [*Penner et al.,* 1998] for carbonaceous aerosol optical thickness would result in a value of 5.6. That would assume, however, that the uncertainties are uncorrelated, which is not the case for the emission and lifetime estimates.

2.3. Other Aerosol Types

Above we described the estimated trend in emissions of aerosols from fossil fuel burning. Additional aerosol types are important for the consideration of the impact of tropospheric aerosol on the radiation balance, since the mixture of different aerosol types determines the aerosol optical properties. The main aerosol types additional to those described above that were taken into account are soil dust, sea salt, natural sulfate, natural organics, and biomass burning aerosol.

Soil dust aerosol is partly a natural aerosol, but part of the dust load in the atmosphere may be originating from anthropogenically disturbed soils; this part may contribute up to 50% to the atmospheric dust load [*Tegen and Fung,* 1995; *Tegen et al.,* 1996]. Dust has a strong interannual variability. Changes in dust sources can be caused by changes in meteorological parameters like surface wind speed and precipitation, as well as in surface conditions like a change in the vegetation cover which protects the soil surface from wind erosion. It has been speculated that interannual variability in dust loads in specific regions may be correlated with climate modes like El Niño - Southern Oscillation [*Prospero and Nees,* 1986] or North Atlantic Oscillation [*Moulin et al.,* 1997], but such relationships have not yet been firmly established. Also, the contribution of disturbed sources to the total dust load is uncertain, and the change in this contribution is undefined. Therefore dust was assumed to be constant during 1950-1990. We used the model-derived distribution from *Tegen and Fung* [1995] to describe the monthly dust distribution for eight different particle size classes between 0.1 and 10 μm and dust optical thickness derived from the concentration and size distribution of the dust, as described by *Tegen and Lacis* [1996].

Sea salt is a natural background aerosol without anthropogenic component, and its mass load is not expected to vary considerably form year to year. Although the concentrations may change regionally with changing wind speeds and precipitation, the source area remains virtually unchanged. To describe the background distribution, the global monthly distribution from *Tegen et al.* [1997] is used, with assuming a higher specific scattering cross section B of 2.5 $m^2 g^{-1}$ following the suggestions by *Quinn and Coffman* [1999] and *Haywood et al.* [1999] for the calculation of sea-salt optical thickness.

Natural sulfate aerosol distribution and optical thickness from DMS emissions has been calculated by *Koch et al.* [1999]. The optical thickness calculation takes into account the particle growth by specific humidity as for the case of anthropogenic sulfate.

Biomass burning aerosol is assumed to be of mainly anthropogenic origin. It also has a strong interannual variability with higher burning during dry years (e.g., Indonesian forest fires during El Niño years) and changes in burning rates. However, due to missing information on these changes we assume this contribution to be constant over the years. We used the monthly biomass burning distribution, as well as the distribution of natural organics from *Liousse et al.* [1996]. Optical thickness was calculated as for the BC and OC aerosols from fossil fuel burning, using specific extinction cross sections B of 9 and 8 $m^2 g^{-1}$, for BC and OC, respectively.

Thus monthly sea-salt, soil dust, natural sulfate, natural organics, and biomass burning aerosol distributions are kept constant over the years 1950 to 1990 but are included in the calculation of global aerosol optical thickness and single-scattering albedo.

3. Total Tropospheric Aerosol Optical Thickness

Plate 1 shows global distributions of the annually averaged optical thicknesses of the individual aerosol types for the year 1990. The differences in the regional distributions indicate that the optical properties of the aerosol mix may vary widely for different regions. From the individual aerosol distributions, the total tropospheric aerosol optical thickness τ was calculated at 0.55 μm wavelength for an external mixture of the tropospheric aerosols. Tropospheric aerosol optical thickness is the sum of the optical thicknesses τ_i of the individual aerosol types, which are summarized for the global annual mean in Table 2. Figure 6 shows the resulting distribution of tropospheric aerosol optical thickness for the years 1950, 1970, and 1990 for the major aerosol types described above, which include natural and anthropogenic sulfate, BC and OC from fossil fuel burning, biomass burning aerosols, natural organics, soil dust and sea salt. Changes in the aerosol optical thickness are caused by changes in fossil fuel emis-

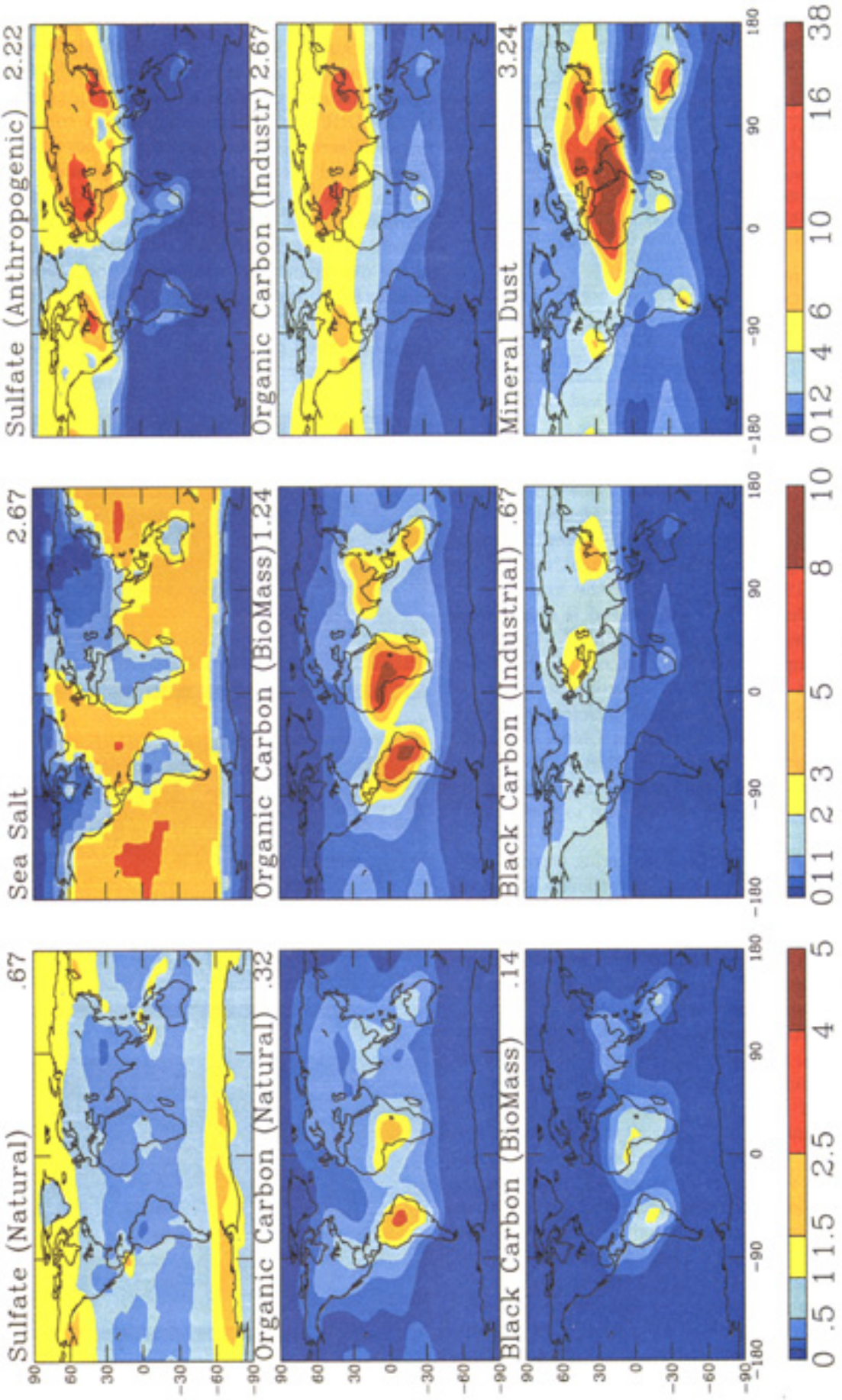

Plate 1. Annually averaged optical thickness (× 100) distributions for the various tropospheric aerosol types for the year 1990.

Table 2. Global Average Optical Thickness, Single-Scattering Albedos at the Reference Wavelength $\lambda = 0.55$ μm, and Nominal Particle Radius for the Individual Aerosol Types

Aerosol Type	Optical Thickness	ω_0	r_{eff}
Sulfate (fossil fuel) 1990	0.004-0.022 (0.011)	1.00	1.0
Sulfate (fossil fuel) 1950	0.002-0.009 (0.005)	1.00	1.0
BC (fossil fuel) 1990	0.001-0.007 (0.003)	0.31	0.1
BC (fossil fuel) 1950	0.000-0.002 (0.001)	0.31	0.1
OC (fossil fuel) 1990	0.-0.027 (0.013)	0.96	0.5
OC (fossil fuel) 1950	0.-0.009 (0.004)	0.96	0.5
Sulfate (natural)	0.007	1.00	0.3
Biomass burning BC	0.001	0.48	0.5
Biomass burning OC	0.012	0.93	1.0
Natural organics	0.003	0.98	0.3
Soil dust	0.032	0.89	[a]
Sea salt	0.027	1.00	2.0

[a]Eight individual size ranges [*Tegen and Lacis*, 1996].

sions. As expected from the emission trend, the optical thickness increased strongly in Asia for this time period. In western Europe, optical thickness increased between 1950 and 1970 and slightly decreased between 1970 and 1990, while in the United States a slight increase is found between 1970 and 1990. For the examples of east Asia and United States this trend is also shown together with the global trend in Figure 7. There the modeled annual optical thicknesses trends are shown for the whole period 1950 to 1990. According to this estimate, the globally averaged optical thickness increased by 0.025 during this period, while in China, the optical thickness nearly doubled. This shift in the global tropospheric aerosol distribution pattern may possibly be causing changes in climate response to the aerosol forcing.

In Figures 8a-8t the modeled scattering aerosol optical thickness is compared to satellite retrievals of aerosol optical thickness from the advanced very high resolution radiometer (AVHRR) [*Rao et al.*, 1988] for the year 1990, which assumes nonabsorbing aerosols in the retrieval algorithm. The retrievals are for ocean areas under clear-sky conditions. We compared modeled and retrieved optical thicknesses for global (ocean) average (Figure 8a) and individual ocean regions (Figures 8b-8t). From such comparisons, no perfect agreement can be expected. Assumptions like spherical particle shape or constant ocean albedo in the retrieval algorithm could cause errors in the satellite optical thickness product, as well as problems with cloud screening. In general, the model results match the retrieved optical thickness well in approximately half of the cases, while overestimating aerosol optical thicknesses (compared to the retrievals) for the other cases. The possible overestimate of the globally averaged ocean optical thickness could be explained by too high sea-salt optical thickness in the model, since we assumed a high specific scattering cross section of 2.5 $m^2 g^{-1}$ for this aerosol type. Thus sea-salt aerosol is the highest contributor to the global averaged ocean aerosol optical thickness. In the North Atlantic (Figures 8b, 8c, and 8d) the high model optical thicknesses are caused by both high sea-salt and organic aerosol optical thicknesses, possibly indicating overestimates of these aerosol types in this region. Since the AVHRR retrievals are for clear-sky conditions, the retrieved aerosol optical thickness values would be underestimated in cases where aerosol plumes are located within or below clouds. This may be the case for the biomass burning plume from South America, which is not observed in the AVHRR retrievals and could result in the discrepancy between model and observations in Figures 8i, 8s, and 8t (this has also been noted by *Tegen et al.* [1997]). Over the Mediterranean and Caspian Seas the highest contribution to modeled aerosol optical

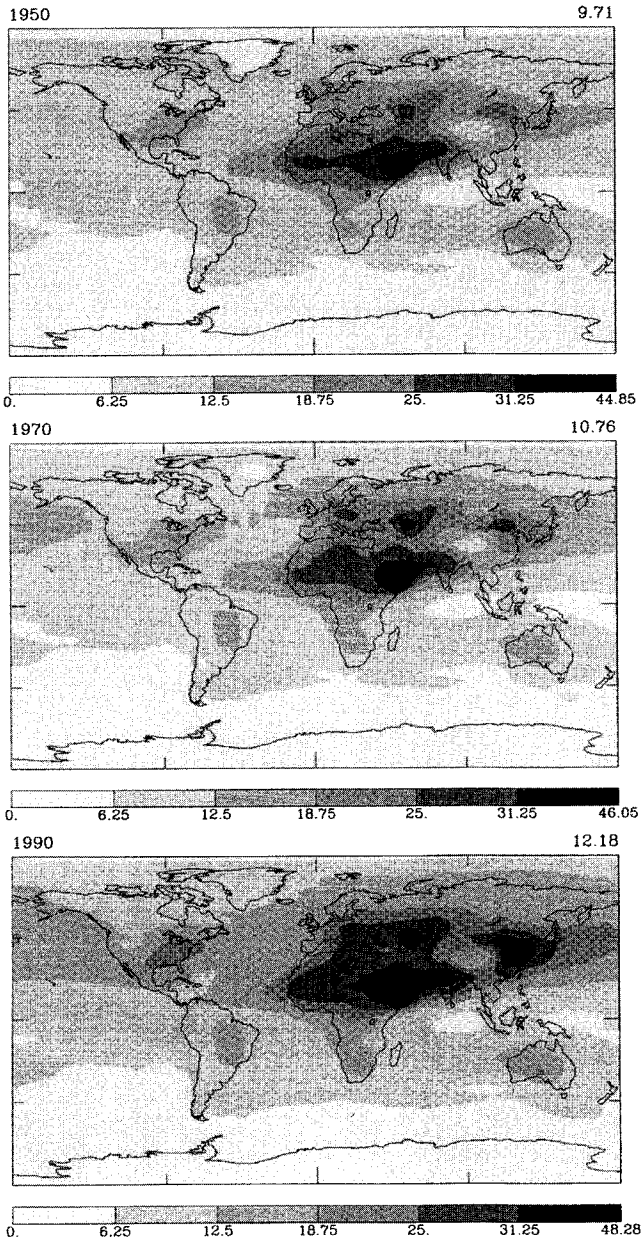

Figure 6. Modeled tropospheric aerosol optical thickness (×100) for the years 1950, 1970, and 1990.

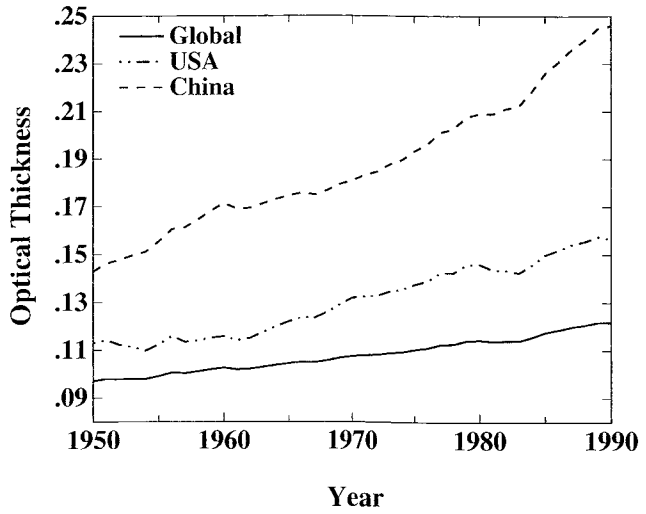

Figure 7. Trend in aerosol optical thickness for fossil fuel sulfate, BC, and OC for the global average and the examples of U.S. and China.

thickness is from dust and sulfate aerosols (presumably dust is overestimated in the model in these regions). In the North Pacific (Figures 8q and 8p) the modeled sulfate optical thicknesses are very high and may be overestimated. Matching of model results with retrieved optical thicknesses could not be achieved at all locations. This comparison indicates regions where either the modeled optical thickness are too high or aerosol optical thickness retrieval is problematic.

4. Single-Scattering Albedo

The tropospheric aerosol single-scattering albedo ω_0 at 0.55 μm wavelength was calculated as

$$\omega_0 = \frac{\sum_{i=1}^{n} \tau_i \omega_{0i}}{\sum_{i=1}^{n} \tau_i}$$

where τ_i and ω_{0i} are the extinction optical thickness and single-scattering albedo of the individual aerosol types, respectively. This calculation included all aerosol types described above and was based on the monthly mean optical thicknesses. The single-scattering albedos for the individual aerosol types that were used for this calculation are summarized in Table 2, together with the global annual average optical thicknesses.

In Figure 9, single-scattering albedos that result from the model are compared to measurements at various locations by different authors, as summarized by *Heintzenberg et al.* [1997]. Additionally shown are values for the recent TARFOX field study off the coast of the northeastern United States [*Hegg et al.,* 1997] and for the Smoke, Clouds, and Radiation-Brazil (SCAR-B) field experiment during burning season in the Brazilian Amazon [*Hobbs et al.,* 1997]. Instead of the aerosol single-scattering albedo of the total atmospheric column, we compared with model results from the first atmospheric layer. Also, since the measurements of single-scattering albedo are generally carried out using dry aerosol [*Heintzenberg et al.,* 1997], we calculated the contribution of sulfate aerosol to the single-scattering albedo without including hygroscopic growth of sulfate particles (this is the only aerosol type for which hygroscopic growth is explicitly taken into account in these calculations). The symbols represent model results for the moderate carbonaceous aerosol case (BC and OC aerosol both 0.5 times the maximum), the error bars indicate the results obtained for maximum-BC (lower limit of the modeled single-scattering albedo) and the low-BC case (upper limit). The results show some spread as can be expected for such a comparison; mostly the moderate-BC case agrees best with the observations. The model results underestimate the observed variability in the single-scattering albedos. Notably, the model considerably overestimates the single-scattering albedo in the Brazilian Amazon during burning season. There the small error bar only indicates the small contribution of fossil fuel aerosol at that location. Since the model produces optical thicknesses that are averaged over a whole month and over a gridbox, the biomass plume is not captured. On the other hand, the model fails to reproduce the very high single-scattering albedos of about 1, which are from measurements at remote regions. Here BC transport in the model may be overestimated. On the other hand, measurements of single-scattering albedo can have large uncertainties as well [*Heintzenberg et al.,* 1997; *Bond et al.,* 1999*a*], which limits the usefulness of such comparisons.

Heintzenberg et al. [1997] also shows results for the latitudinal change in single-scattering albedo during the RITS88 cruise in March 88 in the central Pacific from Dutch Harbor, Alaska, to Samoa. They observed minimum single-scattering albedo of $\approx$ 0.92 at $\approx$ 45°N, which increases to values of $\approx$ 1.0 around 5°N to 10°S. In the model, the minimum single-scattering albedo of 0.93 occurs around 25°N, the values increase to 0.99 at the equator. While the modeled minimum and maximum single-scattering albedo in this part of the globe agrees quite well with the observations, the location of the minimum is located further south than in the real world, reflecting some differences in the atmospheric transport.

Figures 10a-10c show the global distribution of single-scattering albedo of all tropospheric aerosols for the year 1990, for the cases of maximum, moderate, and low carbonaceous aerosol contribution. The global and annual averaged single-scattering albedo for these cases is 0.934, 0.945, and 0.954, respectively. Regions of low single-scattering albedo (as low as 0.89 in some locations in the annual mean) are determined mainly by the BC and soil dust aerosol distributions. In the case of soil dust, the single-scattering albedo of average 0.89 is uncertain and may actually be underesti-

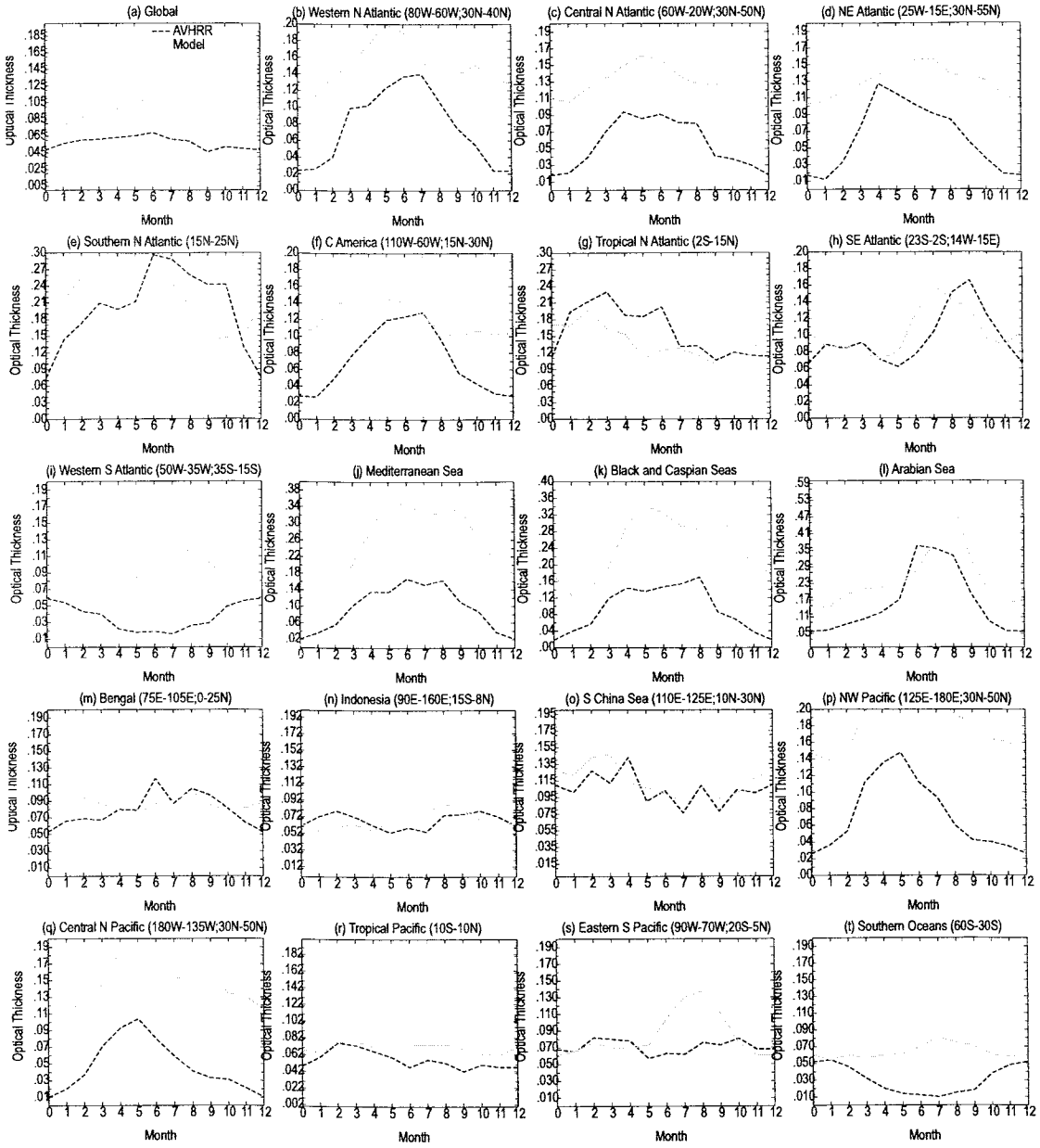

Figure 8. Comparison of modeled tropospheric aerosol optical thickness and the satellite retrieved optical thickness product from NOAA AVHRR [*Rao et al.*, 1988].

mated in several locations. Over the southern oceans the single-scattering albedo is as high as 0.99 since major sources of absorbing aerosols are absent. At high-latitude regions near the North and South Pole the single-scattering albedo decreases, since the more reflecting sulfate aerosols are more efficiently removed during transport than the more absorbing carbonaceous aerosols.

Between the years 1950 and 1990, the results show a slight decrease in global average and U.S. average single-scattering albedos, while a slight increase is obtained for single-scattering albedos in east Asia. However, since the contribution and change in absorbing aerosol is very uncertain, this change is not significant.

5. Aerosol Radiative Forcing

The radiative effect of the tropospheric aerosol distributions described above was calculated by using the radiation model that is embedded in the GISS GCM [*Hansen and Travis,* 1974; *Hansen et al.,* 1983; *Lacis and Mishchenko,* 1995]. Radiative properties (extinction efficiency and asymmetry parameter, in addition to single-scattering albedo) depend on effective particle size and wavelength-dependent complex refractive indices. They were calculated for the standard Γ size distribution with the effective variance 0.2 for each particle type using a Mie scattering algorithm. Refractive indices used here were from measurements of ammonium

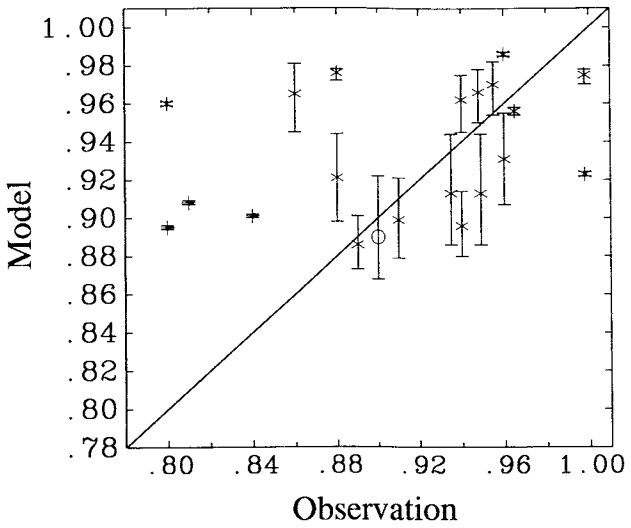

Figure 9. Comparison of modeled tropospheric aerosol single-scattering albedo with Northern Hemisphere measurements summarized by *Heintzenberg et al.* [1997] (asterisks), from TARFOX [*Hegg et al.*, 1997] (open circle), and from SCAR-B [*Hobbs et al.*, 1997] (pluses). The error bars indicate the range obtained for the maximum and low fossil fuel carbonaceous aerosol cases.

sulfate by *Toon et al.* [1976] for sulfate aerosol, measurements of soot aerosol and sea salt [*Nilsson*, 1979] for BC and sea-salt aerosol, respectively, and soil dust measurements by *Patterson et al.* [1977] and *Volz* [1973]. For organic aerosol, the wavelength-dependent refractive indices of ammonium sulfate by *Toon et al.* [1976] was used, with the single-scattering albedo limited to 0.96 for fossil fuel derived organic aerosols, 0.98 for natural organics, and 0.93 for organic aerosols from biomass burning. Reflection, absorption, and transmission of the different aerosol types are calculated using the single Gauss point doubling/adding radiative transfer model in the GISS GCM, with using the correlated K distribution method to compute absorption by gases and particles for six solar and 25 thermal intervals.

Instantaneous radiative forcing and changes in atmospheric heating due to tropospheric aerosols were calculated for nine cases that are summarized in Table 3. Included are the annual and global averages of aerosol optical thickness and single-scattering albedo. Radiative forcing was calculated for the years 1950 to 1990 for the case of "moderate" carbonaceous aerosol contribution (cases FF 90 - FF 50), together with test cases where the contribution of carbonaceous aerosol was maximum (Max C), and the case of "low" carbonaceous aerosol (Min C), as well as for the case of maximum and minimum aerosol optical thickness (Max τ and Min τ). Those latter cases were constructed by choosing the maximum and minimum sulfate aerosol optical thicknesses that are resulting from maximum and minimum SO_2 emissions, together with maximum and minimum contributions of organic aerosols. The minimum contribution of fossil fuel derived organic aerosols was assumed to be zero, since the uncertainties in the loads of this aerosol type are very high. For these maximum and minimum optical thickness cases, the fossil fuel black carbon contributions were chosen to have a value which resulted in a global annual average single-scattering albedo for all tropospheric aerosols of 0.945, which is the same value as the case of moderate black carbon contribution. This condition requires 0.72 and 0.42 times the maximum-BC optical thickness for the maximum and minimum optical thickness case, respectively. In addition to the average forcings for the fos-

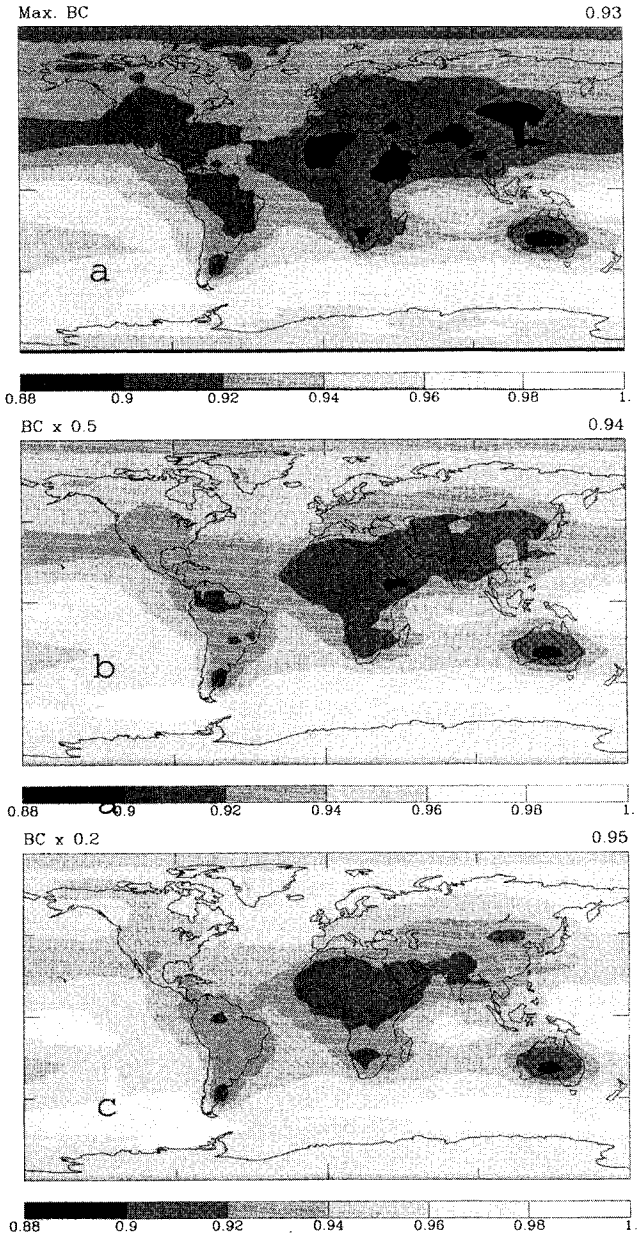

Figure 10. Global distributions of annual averaged single-scattering albedos for the cases of maximum, moderate, and low contribution of fossil fuel carbonaceous aerosols.

Table 3. Radiative Forcing Results for Different Aerosol Scenarios[a]

Scenario	Year	BC/OC % Maximum	Optical Thickness (Fossil Fuel Aerosol)	ω_0 (All Aerosol)	TOA Forcing, $W m^{-2}$	Atmospheric Heating, $W m^{-2}$
FF 90	1990	50	0.039	0.945	-0.27	1.4
FF 80	1980	50	0.029	0.948	-0.24	0.91
FF 70	1970	50	0.024	0.949	-0.19	0.67
FF 50	1950	50	0.014	0.949	-0.10	0.38
Max C	1990	50	0.056	0.934	0.12	2.3
Min C	1990	50	0.029	0.954	-0.51	0.80
Max τ	1990	[b]	0.064	0.945	-0.38	1.8
Min τ	1990	[c]	0.024	0.945	-0.15	0.77
All A	1990	50	0.069	0.945	0.05	2.48

[a]Except All A, all cases are for fossil fuel derived aerosols. All A includes biomass burning aerosols and anthropogenic soil dust (assuming 50% of soil dust to be of anthropogenic origin [*Tegen and Fung*, 1995]).
[b]Sulfate maximum, OC maximum, BC 72% of maximum value.
[c]Sulfate minimum, OC zero, BC 42% of maximum value.

sil fuel aerosol scenarios, we also calculated the TOA forcing and atmospheric heating caused by all anthropogenic aerosols (including biomass burning and anthropogenic dust, case "all A"). Those calculations were carried out for the moderate case for the year 1990. The radiative forcing was calculated by running the GISS GCM for one model year without the specified aerosol distribution. It was then rerun for the model year with the different aerosol scenarios, with the atmospheric circulation and cloud optical properties and water vapor prescribed by the no-aerosol experiment. The instantaneous forcing was calculated as the difference between the modeled radiative fluxes with the different aerosol scenarios and the no-aerosol experiment.

6. Results

The global average values for changes in TOA radiative fluxes and radiative heating for the different aerosol scenarios are summarized in Table 3. Atmospheric heating (calculated as the difference between TOA and surface forcing) shows the amount of energy absorbed in the atmospheric column due to the instantaneous forcing. The fossil fuel aerosol optical thickness increased substantially from 0.014 to 0.039 from the years 1950 to 1990 (FF 50 - FF 90). The optical thickness of the sum of all tropospheric aerosols increased from 0.097 to 0.122 over this period, while the globally averaged single-scattering albedo decreased slightly. The change in the globally averaged optical thickness over the four decades (an increase of 0.025 from 1950 to 1990) is smaller than the difference for the maximum and minimum optical thickness scenarios, but in addition to the changes in the global average numbers the regional distribution of the fossil fuel derived aerosols shifted considerably over this time period.

Changes in fossil fuel aerosol from 1950 to 1990 cause a decrease by ≈ 0.2 Wm^{-2} in negative TOA radiative forcing and an increase in atmospheric heating by ≈ 1 Wm^{-2} (cases FF 50 to FF 90). The relatively small numbers for TOA forcings are caused by cancellation

Table 4. Comparison of Estimates of TOA Aerosol Radiative Forcing by Mixtures of Sulfate and Carbonaceous Aerosols[a]

Reference	OC Included	Biomass Burning Included	TOA Forcing ($W m^{-2}$)	Comment
Haywood et al. [1997]	no	no	–0.18	
Haywood et al. [1997]	no	no	+0.02	internal mixture
Mhyre et al. [1999]	no	no	–0.16	
Mhyre et al. [1999]	no	no	–0.10	internal mixture
Schult et al. [1997]	no	yes	–0.2	
Haywood and Ramaswamy [1998]	no	yes	–0.4	
Cooke et al. [1999]	yes	no	+0.15	no sulfate
This work	yes	no	–0.51 - +0.12	
Penner et al. [1998]	yes	no	–0.65 - –0.35	
Penner et al. [1998]	yes	yes	–0.88 - –0.49	
Penner et al. [1998]	yes	yes	–0.75 - –0.30	internal mixture
Hansen et al. [1998]	yes	yes	–0.42	
Haywood et al. [1999]	yes	yes	–1.57	clear-sky only

[a]If not noted otherwise, the calculations were for external aerosol mixtures.

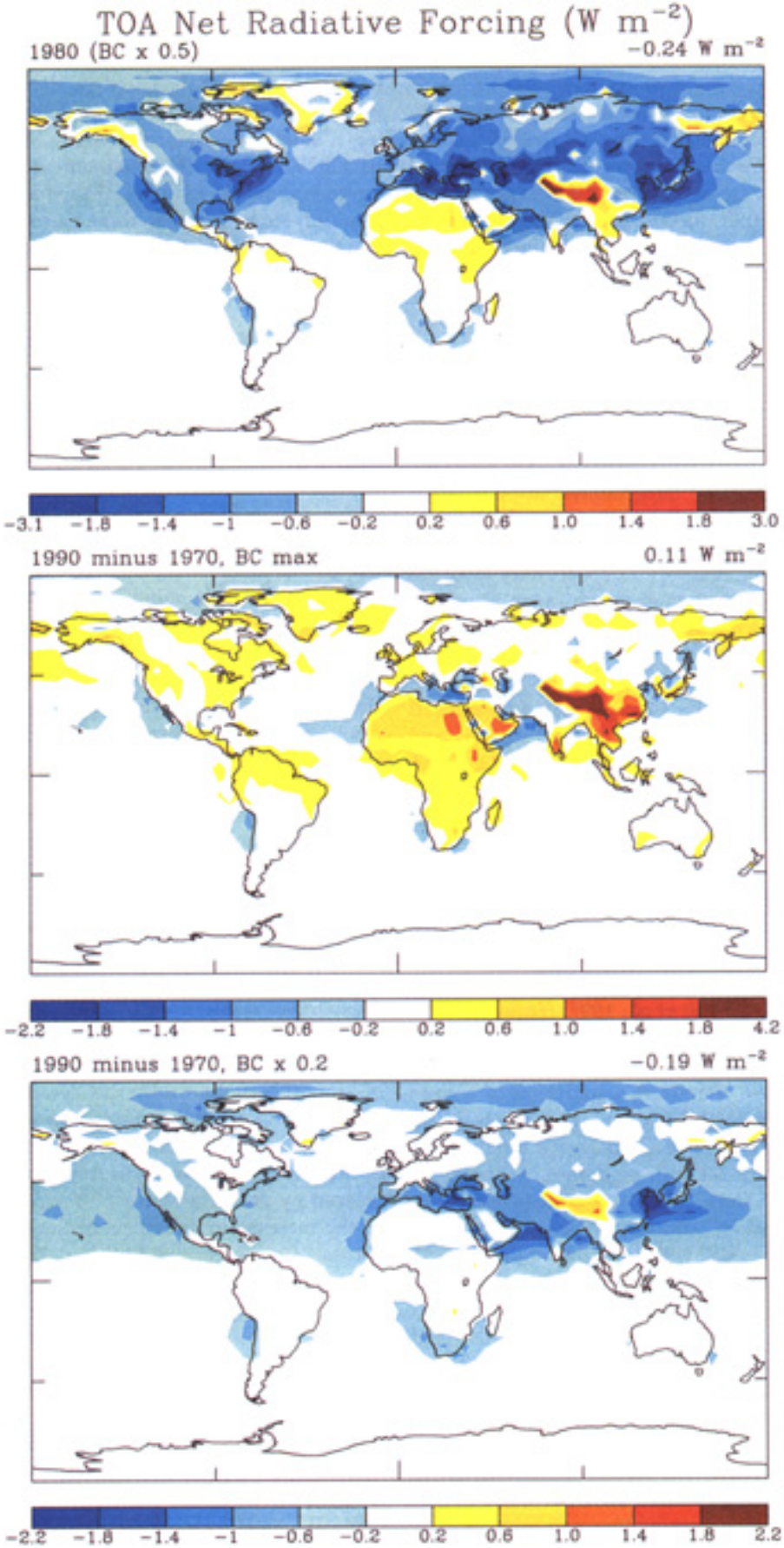

Plate 2. Net TOA radiative forcing (Wm^{-2}) (a) for 1980 for moderate fossil fuel carbonaceous aerosol contribution, (b) the change between 1970 and 1990 occurring for the cases of maximum and (c) low fossil fuel carbonaceous aerosol.

of positive and negative solar forcing values over bright and dark surfaces in the global average.

The large uncertainty in aerosol single-scattering albedo leads to the high uncertainty in the forcing estimates. The differences between the maximum and minimum BC cases are ≈ 0.6 Wm^{-2} for TOA forcings and 1.5 Wm^{-2} in atmospheric heating. The differences between the maximum and minimum optical thickness cases is less, ≈ 0.2 Wm^{-2} for TOA forcings and 1 Wm^{-2} for the atmospheric heating. In contrast to the fossil fuel aerosol cases, the TOA forcing is positive for the case where all anthropogenic aerosols are considered (All A). The positive forcing in this case is due to the contribution of absorbing biomass burning and dust aerosol over bright desert surfaces, together with the contribution of thermal forcing from the large dust aerosols. Additional large uncertainties are connected with the estimates of those additional anthropogenic aerosol types. The range of forcings from these scenarios are given in place of a formal uncertainty analysis, which cannot be given since even the range in optical parameters for some of the aerosol types is unknown.

The aerosol radiative effect was calculated by treating the aerosols as an external mixture. According to *Haywood and Shine* [1995], the absorption due to aerosols increases for an internal mixture of black carbon and sulfate, which could cause a 20-60% decrease in TOA forcing.

The resulting range in TOA forcings considering the uncertainties in the aerosol distribution and optical properties agrees with the range of TOA forcings of other recent investigations of mixtures of sulfate and carbonaceous aerosols, which are summarized in Table 4. Several studies found global average TOA forcing values for mixtures of BC and sulfate aerosols that lie within a close range [*Schult et al.,* 1997; *Haywood et al.,* 1997; *Mhyre et al.,* 1999]. The close agreement between the latter two studies may not be that surprising, since both made the simplified assumption of a fixed ratio of 0.075 between BC and sulfate aerosols. *Penner et al.* [1998] find a stronger negative forcing than our reference case FF 90 with moderate carbonaceous aerosols. They also show changes in atmospheric heating due to fossil fuel BC and OC; their resulting value of 0.92 Wm^{-2} agrees well with the value of 0.91 Wm^{-2} we obtain for the moderate-BC fossil fuel aerosol distribution for the year 1980 (FF 80).

Differences in the global average values for TOA forcings do not necessarily reflect differences in the regional forcings, since regional changes in positive and negative forcings may cancel if globally averaged, resulting in a small global mean forcing. Plate 2a shows the regional distribution of the TOA net forcing due to industrial aerosols for the year 1980, which shows that in this case the forcing is mostly negative. Plates 2b and 2c show the changes in forcing between the years 1970 and 1990 for the cases of maximum and minimum contribution of carbonaceous aerosols. Depending on the assumptions about the contribution of absorbing aerosol, the average forcing either increased or decreased during that period. While the change in global mean TOA forcing is small, the regional increase in forcing can be up to 4.2 W m^{-2} for the maximum BC and -2.1 W m^{-2} for the minimum-BC case. The change in global mean atmospheric heating for these cases can also vary substantially between -0.4 and 1.2 W m^{-2} for the period 1970 to 1990 for the extreme cases of BC contribution.

7. Conclusions

There is little doubt that the presence of strongly absorbing (black carbon) aerosol decreases the negative TOA aerosol direct radiative forcing compared to the forcing by sulfate aerosol alone. However, there is considerable uncertainty in those estimates, which limits the usefulness of radiative forcing estimates for climate studies, until they are further constrained. While we can give some estimates of uncertainties that are caused by uncertainties in input parameters and model processes, there are additional uncertainties that are not known. Those uncertainties can be caused by mechanisms like aging of particles that are not included in the model, or by subgrid scale variations that are not resolved. For the parametric uncertainties that were considered here we find that in the case of fossil fuel derived aerosols, the largest uncertainty is due to emission factors of carbonaceous aerosol. This parameter has an uncertainty factor of approximately 4, compared to the smaller uncertainty factors for sulfur emissions and the optical properties of sulfate and carbonaceous aerosol species, which are of the order of 1-2. To reduce the uncertainties in emission factors of carbonaceous aerosols, more measurements of such emission factors for different types of burning are needed, which should be specifically tailored for use in climate studies.

In addition to the uncertainties in optical properties of tropospheric aerosols, the decadal change in their distribution should be taken into account for climate change studies. For the period 1950 to 1990, the global optical thickness of aerosols from fossil fuel burning increased by nearly a factor of 3 according to estimates of the increase in emissions of SO_2 and carbonaceous aerosols from fossil fuel burning. Due to this increase, the total tropospheric aerosol optical thickness (including natural aerosols) increased by about 25% over this period. While this number is relatively small considering the overall uncertainties, there was also a significant shift in the regional aerosol distribution. In east Asia, the aerosol optical thickness increase was especially strong due to the increase in fossil fuel emissions, while in the United States and western Europe, SO_2 emissions leveled since the early 1980s due to emission controls. (Advances in filter technology which would lead to a decrease of particle emissions for carbonaceous aerosols have not been considered in these estimates.) Although we can estimate this regional shift in fossil

fuel derived aerosol optical thickness with some confidence, the change in single-scattering albedo (which determines the change in TOA radiative forcing and the sign of this forcing) remains unclear. The decadal changes in aerosol optical thickness magnitudes and shifts in regional distributions result in changes in global direct aerosol radiative forcing, which are of the same magnitude as the uncertainties in forcing due to uncertainties in total optical thickness.

We regard these time dependent model-derived tropospheric aerosol distributions as a first step toward a climatology that is useful for climate change studies. We expect that it will be improved and updated by inputs from the scientific community. Some constraint of the aerosol forcing and decadal trends will be obtained by a comparison with long-term surface radiation observations.

Acknowledgments. The authors would like to thank J. Hansen, B. Liepert, and T. Bond for fruitful discussions. Suggestions from three anonymous reviewers helped to substantially improve an earlier version of the manuscript. This work was partly supported by the NASA Earth Science Enterprise program (NASA grant NAG5-4052), the Global Aerosol Climatology Project managed by R. Curran ans the NASA ACMAP EOS/IDS project on Chemistry, Aerosols, and Climate (CACTUS) IDS.

References

Benkovitz, C. M., T. Scholtz, J. Pacyna, L. Tarrason, J. Dignon, E. C. Voldner, P. A. Spiro, J. A. Logan, and T. E. Graedel, Global gridded inventories of anthropogenic emissions of sulfur and nitrogen, *J. Geophys. Res.*, *101*, 29,239–29,253, 1996.

Boden, T. A., G. Marland, and R. J. Andres, Estimates of global, regional, and national annual CO_2 emissions from fossil-fuel burning, hydraulic cement production, and gas flaring: 1950-1992, Tech. Rep. *ORNL/CDIAC-90, NDP-030/R6*, 600 pp., Oak Ridge Natl. Lab., Oak Ridge, Tenn., 1996.

Bond, T. C., R. Charlson, and J. Heintzenberg, Quantifying the emission of light-absorbing particles: Measurements tailored to climate studies, *Geophys. Res. Lett.*, *25*, 337–340, 1998.

Bond, T. C., T. L. Anderson, and D. Campbell, Calibration and intercomparison of filter-based measurements of visible light absorption by aerosols, *Aerosol Sci. Technol.*, *30*, 582–600, 1999a.

Bond, T. C., M. Bussemer, B. Wehner, S. Keller, R. J. Charlson, and J. Heintzenberg, Light absorption by primary particle emissions from a lignite burning plant, *Environ. Sci. Technol.*, *33*, 3887–3891, 1999b.

Charlson, R. J., D. S. Covert, and T. V. Larson, Observation of the effect of humidity on light scattering by aerosols, in *Hygroscopic Aerosols*, edited by L. R. and A. Deepak, pp. 35–44, A. Deepak, Hampton, Va., 1984.

Charlson, R. J., J. Langner, H. Rodhe, C. B. Leovy, and S. G. Warren, Perturbation of the Northern Hemisphere radiative balance by backscattering from anthropogenic sulfate aerosols, *Tellus*, *43AB*, 152–163, 1991.

Cooke, W. F., and J. N. Wilson, A global black carbon aerosol model, *J. Geophys. Res.*, *101*, 19,395–19,409, 1996.

Cooke, W. F., C. Liousse, H. Cachier, and H. Feichter, Construction of a $1° \times 1°$ fossil fuel emission data set for carbonaceous aerosol and implementation and radiative impact in the ECHAM4 model, *J. Geophys. Res.*, *104*, 22,137–22,162, 1999.

Dignon, J., and S. Hameed, Global emissions of nitrogen and sulfur oxides from 1860 to 1980, *J. Air Pollut. Control Assoc.*, *39*, 180–186, 1989.

Hansen, J. E., and L. D. Travis, Light scattering in planetary atmospheres, *Space Sci. Rev.*, *16*, 527–610, 1974.

Hansen, J. E., G. L. Russell, D. Rind, P. Stone, A. Lacis, S. Lebedeff, R. Ruedy, and L. Travis, Efficient three–dimensional global models for climate studies: Models I and II, *Mon. Weather Rev.*, *111*, 609–662, 1983.

Hansen, J. E., M. Sato, and R. Ruedy, Radiative forcing and climate response, *J. Geophys. Res.*, *102*, 6831–6864, 1997.

Hansen, J. E., M. Sato, A. Lacis, R. Ruedy, I. Tegen, and E. Matthews, Climate forcings in the industrial era, *Proc. Natl. Acad. Sci. U.S.A.*, *22*, 12,753–12,758, 1998.

Haywood, J. M., and V. Ramaswamy, Global sensitivity studies of the direct radiative forcing due to anthropogenic sulfate and black carbon aerosols, *J. Geophys. Res.*, *103*, 6043–6058, 1998.

Haywood, J. M., and K. P. Shine, The effect of anthropogenic sulfate and soot aerosol on the clear sky planetary radiation budget, *Geophys. Res. Lett.*, *22*, 603–606, 1995.

Haywood, J. M., D. L. Roberts, A. Slingo, J. M. Edwards, and K. P. Shine, General circulation model calculations of the direct radiative forcing by anthropogenic sulfate and fossil fuel soot aerosols, *J. Clim.*, *10*, 1562–1577, 1997.

Haywood, J. M., V. Ramaswamy, and B. J. Soden, Tropospheric aerosol forcing in clear-sky satellite observations over the oceans, *Science*, *283*, 1299–1303, 1999.

Hegg, D. A., J. Livingston, P. V. Hobbs, T. Novakov, and P. Russel, Chemical apportionment of aerosol column optical depth off the mid-Atlantic coast of the United States, *J. Geophys. Res.*, *102*, 25,293–25,303, 1997.

Heintzenberg, J., R. J. Charlson, A. D. Clarke, C. Liousse, V. Ramaswamy, K. P. Shine, M. Wendisch, and G. Helas, Measurements and modelling of aerosol single scattering albedo: Progress, problems and prospects, *Beitr. Phys. Atmos.*, *70*, 249–263, 1997.

Hobbs, P. V., J. S. Reid, R. A. Kotchenruther, R. J. Ferek, and R. Weiss, Direct radiative forcing by smoke from biomass burning, *Science*, *275*, 1776–1778, 1997.

Hollrigl, P., Modelling the distribution of aerosols and their effect on the atmospheric radiation, Ph.D. thesis, Eidg. Tech. Hochsch. Zürich, Switzerland, 1997.

Kiehl, J. T., and B. P. Briegleb, The relative importance of sulfate aerosols and greenhouse gases in climate forcing, *Science*, *260*, 311–314, 1993.

Kiehl, J. T., and H. Rodhe, Modeling geographical and seasonal forcing due to aerosols, in *Aerosol Forcing of Climate*, edited by R. Charlson and J. Heintzenberg, pp. 281–296, John Wiley, New York, 1995.

Koch, D., D. Jacob, I. Tegen, D. Rind, and M. Chin, Tropospheric sulfur simulation and sulfate direct radiative forcing in the GISS GCM, *J. Geophys. Res.*, *104*, 23,799–23,822, 1999.

Lacis, A. A., and M. I. Mishchenko, Climate forcing, climate sensitivity, and climate response: A radiative modeling perspective on atmospheric aerosols, in *Aerosol Forcing of Climate*, edited by R. Charlson and J. Heintzenberg, pp. 11–42, John Wiley, New York, 1995.

Lavanchy, V., H. W. Gäggeler, U. Schotterer, M. Schwikowski, and U. Baltensperger, Historical record of carbonaceous particle concentrations from a European high-alpine glacier (Colle Gnifetti, Switzerland), *J. Geophys. Res.*, *104*, 21,227–21,237, 1999.

Lefohn, A. S., J. D. Husar, and R. B. Husar, Estimating historical anthropogenic global sulfur emission patterns for the period 1850-1990, *Atmos. Environ.*, *33*, 3435–3444, 1999.

Liousse, C., J. E. Penner, C. Chuang, J. J. Walton, H. Eddleman, and H. Cachier, A global three-dimensional model study of carbonaceous aerosols, *J. Geophys. Res.*, *101*, 19,411–19,432, 1996.

Malm, W. C., J. F. Sisler, D. Huffman, R. A. Eldred, and T. A. Cahill, Spatial and temporal trends in particle concentration and optical extinction in the United States, *J. Geophys. Res.*, *99*, 1347–1370, 1994.

Mayewski, P. A., W. B. Lyons, M. J. Spencer, M. S. Twickler, C. F. Buck, and S. Whitlow, An ice core record of atmospheric response to anthropogenic sulphate and nitrate, *Nature*, *346*, 554–556, 1990.

Mhyre, G., F. Stordal, K. Restad, and I. S. A. Isaaksen, Estimates of the direct radiative forcing due to sulfate and soot aerosols, *Tellus*, *50B*, 463–477, 1999.

Mosher, B. W., P. Winkler, and J. L. Jaffrezo, Seasonal aerosol chemistry at Dye 3, Greenland, *Atmos. Environ.*, *27*A, 2761–2772, 1993.

Moulin, C., C. E. Lambert, F. Dulac, and U. Dayan, Control of atmospheric export of dust from North Africa by the North Atlantic Oscillation, *Nature*, *387*, 691–694, 1997.

National Acid Deposition Program National Trends Network (NRSP-3), tech. rep. NADP Program Off., Ill. State Water Surv., Champaign, 1999.

Nilsson, B., Meteorological influence on aerosol extinction in the 0.2–40 μm wavelength range, *Appl. Opt.*, *18*, 3457–3473, 1979.

Patterson, E. M., D. A. Gillette, and B. H. Stockton, Complex index of refraction between 300 and 700 nm for Saharan aerosols, *J. Geophys. Res.*, *82*, 3153–3160, 1977.

Penner, J. E., R. J. Charlson, J. M. Hales, N. S. Laulainen, R. Leifer, T. Novakov, J. Ogren, L. F. Radke, S. E. Schwartz, and L. Travis, Quantifying and minimizing uncertainty of climate forcing by anthropogenic aerosols, *Bull. Am. Meteorol. Soc.*, *75*, 375–400, 1994.

Penner, J. E., C. C. Chuang, and K. Grant, Climate forcing by carbonaceous and sulfate aerosols, *Clim. Dyn.*, *14*, 839–851, 1998.

Prospero, J. M., and R. T. Nees, Impact of the North African drought and El Niño on mineral dust in the Barbados trade winds, *Nature*, *320*, 735–738, 1986.

Quinn, P. K., and D. J. Coffman, Comment on "Contribution of different aerosol species to the global aerosol extinction optical thickness: Estimates from model results" by Tegen et al., *J. Geophys. Res. 104*, 4241–4248, 1999.

Rao, C. R. N., L. L. Stowe, E. P. McClain, J. Sapper, and M. P. McCormick, Development and application of aerosol remote sensing with AVHRR data from the NOAA satellites, in *Aerosols and Climate*, edited by P. V. Hobbs, pp. 69–79, A. Deepak, Hampton, Va., 1988.

Roeckner, E., T. Siebert, and J. Feichter, Climatic response to anthropogenic sulfate forcing simulated with a general circulation model, in *Aerosol Forcing of Climate*, edited by R. Charlson and J. Heintzenberg, pp. 349–362, John Wiley, New York, 1995.

Schaug, J., J. Hansen, K. Nodop, B. Ottar, and J. M. Pacyna, Summary report from the chemical coordinating center for the third phase of EMEP, *Tech. Rep. EMEP/CC Rep. 3/87*, 160pp., Norw. Inst. for Air Res., Lillestrom, 1987.

Schult, I., J. Feichter, and W. F. Cooke, Effect of black carbon and sulfate aerosols on the global radiation budget, *J. Geophys. Res.*, *102*, 30,107–30,117, 1997.

Schwikowski, M., A. Döscher, H. W. Gäggeler, and U. Schotterer, Anthropogenic versus natural sources of atmospheric sulfate from an Alpine ice core, *Tellus*, *51B*, 938–951, 1999a.

Schwikowski, M., S. Brütsch, H. G. Gäggeler, and U. Schotterer, A high-resolution air chemistry record from an Alpine ice core: Fischerhorn glacier, Swiss Alps, *J. Geophys. Res.*, *104*, 13,709–13,720, 1999b.

Tegen, I., and I. Fung, Modeling of mineral dust in the atmosphere: Sources, transport, and optical thickness, *J. Geophys. Res.*, *99*, 22,897–22,914, 1994.

Tegen, I., and I. Fung, Contribution to the mineral

aerosol load from land surface modification, *J. Geophys. Res.*, *100*, 18,707–18,726, 1995.

Tegen, I., and A. A. Lacis, Modeling of particle size distribution and its influence on the radiative properties of mineral dust aerosol, *J. Geophys. Res.*, *101*, 19,237–19,244, 1996.

Tegen, I., A. Lacis, and I. Fung, The influence of mineral aerosol from disturbed soils on the global radiation budget, *Nature*, *380*, 419–422, 1996.

Tegen, I., P. Hollrigl, M. Chin, I. Fung, D. Jacob, and J. Penner, Contribution of different aerosol species to the global aerosol extinction optical thickness: Estimates from model results, *J. Geophys. Res.*, *102*, 23,895–23,915, 1997.

Toon, O. B., J. B. Pollack, and B. N. Khare, The optical constants of several atmospheric aerosol species: Ammonium sulfate, aluminum oxide, and sodium cloride, *J. Geophys. Res.*, *81*, 5733–5748, 1976.

United Nations, The United Nations Energy Statistica Database (1994), technical report, United Nations Statistics Division, 1996.

Volz, F. E., Infrared optical constants of ammonium sulfate, Sahara dust, volcanic pumice, and flyash, *Appl. Opt.*, *12*, 564–568, 1973.

D. Koch and M. Sato, Center for Climate Systems Research, Columbia University and NASA Goddard Institute for Space Studies, 2880 Broadway, New York, NY 10025.

A. Lacis, NASA Goddard Institute for Space Studies, 2880 Broadway, New York, NY 10025.

I. Tegen, Max-Planck-Institute for Biogeochemistry, P.O. Box 100164, 07701 Jena, Germany. (itegen@bgc-jena.mpg.de)

(Received September 3, 1999; revised April 26, 2000; accepted April 30, 2000.)